ELSEVIER

Earth and Planetary Science Letters 201 (2002) 69–86

EPSL

www.elsevier.com/locate/epsl

Low water contents in pyroxenes from spinel-peridotites of the oxidized, sub-arc mantle wedge

Anne H. Peslier *, James F. Luhr, Jeffrey Post

Department of Mineral Sciences, NHB-119, Smithsonian Institution, Washington, DC 20560, USA

Received 2 November 2001; received in revised form 10 April 2002; accepted 10 April 2002

Abstract

Pyroxene water contents measured by Fourier transform infrared spectrometry for Mexican and Simcoe (WA, USA) spinel-peridotite xenoliths range from 140 to 528 ppm in clinopyroxenes and 39 to 265 ppm in orthopyroxenes. Correlations between these water contents and major-element compositional data for the pyroxenes, associated spinels, and whole-rock xenoliths demonstrate that these water contents record mantle values that have not been perturbed since the xenoliths were brought to the surface by their host magmas. Broad positive correlations of pyroxene water contents with whole-rock Al_2O_3 are consistent with water behaving as an incompatible element during peridotite melting. The main control on the range of pyroxene water contents, however, appears to be the redox state of the peridotite, because estimates of oxygen fugacity from Mössbauer (Simcoe) and microprobe data (Mexico) on spinels are negatively correlated with water contents. This is consistent with the dominant mechanism of H incorporation into pyroxene, which is dependent on the oxidation-reduction of iron. Metasomatism of sub-arc mantle-wedge peridotites by oxidized fluids or melts rising from the slab raises the oxygen fugacity of the peridotites, and where temperature is high enough, induces them to partially melt. The oxidation, in turn, lowers the solubility of water in the peridotite minerals, causing more than half of the original water to be expelled. That water enters the hydrous partial melts and these ascend through the lithosphere to feed the arc magmatic system in the upper crust. Low water contents in pyroxenes from sub-arc mantle-wedge peridotites, such as those from Simcoe and some western Mexican sites, therefore appear to be complementary to the high water contents that characterize subduction-zone magmas and fuel their explosive eruptions. An estimate of water budget in subduction zones, however, indicates that the amount of water coming from the dehydration of mantle-wedge anhydrous minerals probably accounts for less than 5% of the total water present in subduction-related magmas. The high water contents of arc magmas thus are mainly attributed to fluids or melts from the slab proper. The relatively dry sub-arc mantle wedge appears to be an effective medium through which subducted water is transported from slabs toward the surface. Published by Elsevier Science B.V.

Keywords: water; Fourier transform infrared spectroscopy; pyroxene group; mantle; xenoliths

1. Introduction

Understanding the effects of a dehydrating subducting slab on the overlying peridotitic mantle wedge may provide the key to deciphering many

* Corresponding author. Present address: Texas Center for Superconductivity (TCS-UH), HSC building, University of Houston, Houston, TX 77204, USA. Tel.: +1-713-743-8283; Fax: +1-713-743-8281.

E-mail address: apeslier@mail.uh.edu (A.H. Peslier).

0012-821X/02/$ – see front matter Published by Elsevier Science B.V.
PII: S0012-821X(02)00663-5

fundamental Earth processes, such as the generation of subduction-zone magmas, slab recycling, mantle convection, and the growth of continents. Considerable mass transfer is thought to take place from the slab into the overlying mantle wedge, through the medium of poorly understood metasomatic fluids or melts [1]. The volatile-rich character of subduction-zone magmas is generally attributed to the relatively shallow ($\sim$90 km) breakdown of amphibole in the slab and upward release of water into the down-dragged base of the mantle wedge [2]. K-rich amphibole, and various dense hydrous magnesium silicates in the slab, however, are capable of carrying subducted water to significantly greater depths, even to the mantle transition zone below 400 km depth [3]. Water-budget calculations suggest that only about 20% of the water carried down by slabs can be accounted for by the water in subduction-zone magmas [1]. Thus, the majority of subducted water must be stored for considerable lengths of time in various parts of the mantle. Possible explanations include a significant presence of hydrous minerals in the down-dragged base of the mantle wedge [2,3], or storage of water in high-pressure hydrous phases in the mantle transition zone [4,5]. Water, or more precisely hydrogen protons, however, can also enter the structures of the dominant upper-mantle minerals olivine, pyroxene, and garnet. Hydrogen is thought to be located in lattice defects in these 'nominally anhydrous' minerals, where it can reach concentrations of several hundred ppm H_2O [6]. The possibility that important quantities of water are stored in these minerals in peridotites of the sub-arc mantle wedge has never been quantitatively addressed.

Knowing the amount of water present in anhydrous minerals from the mantle wedge has potential bearing upon the entire cycle of hydrogen in the Earth. Water can also affect many physical and chemical properties of that part of the mantle. For example, trace amounts of water in peridotite minerals can lower their mechanical strength [7,8], increase the internal rate of ionic diffusion [9], enhance mantle electrical conductivity [10], reduce seismic-wave velocities [11], and change phase relations and melt compositions [12–14]. Therefore, knowledge of the amount of water in the main phases of the mantle, a crucial part of which is located above subduction zones, is key to constraining many essential parameters for understanding mantle geodynamics.

The purpose of this paper is to present Fourier transform infrared (FTIR) data used to determine pyroxene water contents from sub-arc mantle-wedge peridotite xenoliths and to compare them to pyroxenes from peridotite xenoliths farther inboard from the continental margin, taken to represent ambient mantle unaffected by subduction. We show that pyroxene water contents in spinel-peridotite xenoliths from Mexico and Simcoe (WA, USA) are mainly controlled by the oxidation state of the mantle, with the mantle wedge being more oxidized than the mantle farther removed from subduction effects.

2. Sample selection and regional geology

The mantle xenoliths used in this study, from Mexico and NW USA (Fig. 1), were brought to the surface by mafic alkalic magmas erupted during Plio–Pleistocene time. They are spinel peridotites characterized by the presence of Cr-diopside, defined as type I by Frey and Prinz [15].

Mexico is an assemblage of different tectonic terranes that progressively accreted to the North American craton from the late Paleozoic to the early Cenozoic [16]. During most of Mesozoic–Cenozoic time, the Farallon plate was subducting eastward beneath western Mexico. Samples were selected from five mantle xenolith locations that span a 1700 km NW–SE transect across the Basin and Range Province of Mexico (Fig. 1). These xenoliths are considered to represent samples of the upper mantle at increasing distances (175–610 km) from the paleotrench to the west [16]. The spinel peridotites are dominantly lherzolites and show a wide range of major element contents at each location, indicating various degrees of melt depletion. Minimum oxygen fugacities estimated from electron microprobe analyses and expressed as ΔFMQ values ($=\log fO_2$ in sample minus log fO_2 for fayalite–magnetite–quartz buffer at the same temperature and pressure) were found to

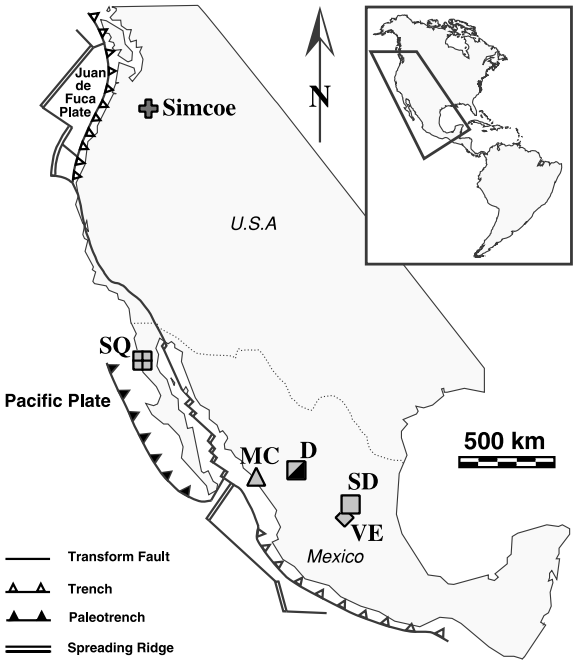

Fig. 1. Map of the western part of North America, showing xenolith locations and current and former plate boundaries in the adjacent Pacific Ocean, broadly taken from [19,55]. Mexican xenolith locations: VE = Ventura–Espíritu Santo, SD = Santo Domingo, D = Durango, MC = Mesa Cacaxta, SQ = San Quintín.

increase from −2.2 in the SE to −0.4 in the NW; variability in ΔFMQ decreases toward the west as well [16]. This increase in mantle oxidation state with proximity to the paleotrench was interpreted as reflecting the enhanced influence of oxidizing metasomatic fluids/melts from the slab on the lithospheric mantle toward the west [16]. Lattard [17], however, has challenged two aspects of this interpretation. She argued that the calculated ΔFMQ values in Mexican xenoliths do not reflect their true oxidation state, and discounts that metasomatism is associated with oxidation.

Simcoe shield volcano (Washington State, USA) is located 200 km north of the northernmost part of the US Basin and Range Province [18], and erupted through Phanerozoic lithosphere. The Farallon plate, now represented by the remnant Juan de Fuca and Gorda plates (Fig. 1), has been subducting eastward beneath the northwestern USA for ~50 Ma [19]. Simcoe xenoliths represent mantle-wedge spinel peridotites collected 65 km east of the Cascade arc. They are harzburgites, and thus record relatively high degrees of melt depletion. Calculated oxygen fugacities based on Mössbauer analyses of spinels are high, with ΔFMQ values of 0–1.8 [20]. As mentioned above for the Mexican case, these oxidized conditions are thought to result from slab-derived oxidizing melts or fluids passing through the mantle wedge [20,21]. U–Th–Pb, Re–Os, and Sm–Nd isotopic studies show that metasomatic fluids/melts from the slab also changed the isotopic characteristics of the Simcoe peridotites during multi-stage processes spanning more than 10 Ma [22,23].

3. Analytical techniques

3.1. Sample preparation

Twenty to 40 grains of both clinopyroxene (diopside) and orthopyroxene (enstatite) were handpicked from each sample with an effort to avoid grains with cracks, fluid, mineral or melt inclusions, and exsolution lamellae. Some samples had ubiquitous fluid inclusions, and these were only investigated if paths free of inclusions could be selected for FTIR analysis. The selected mineral grains were mounted in EPO-TEK 301 epoxy on a 2.5 cm circular glass slide. The mount was then ground with an Ingram thin-section grinder until the surface of each mineral grain was exposed. Polishing involved two steps: (1) on a TEXMET 1000 polishing cloth with 6 μm Glenel Corporation Grade-15 diamond compound and ethylic glycol lubricant; (2) on a 600 grit alumina oxide polishing cloth with 0.5 μm alumina abrasive. The polished surface was attached to a new glass slide with Crystalbond thermoplastic, and the first glass slide was ground away. Grinding continued until the second surface of each mineral grain was exposed. This second surface was then polished as described above. The doubly polished wafer was detached from the glass slide by heating the Crystalbond on a hotplate, and finally by soaking the wafer in acetone for a few minutes with ultrasonic agitation.

Mineral orientation was determined by observation of interference figures using a petrographic microscope. Grains that showed Bxo, Bxa, or optic-normal figures were photographed in plane transmitted light and the principal axes of the optical indicatrix were labeled based on the interference figure. Thickness was measured on each suitably oriented grain with an ID-C 543 Mitutoyo digital micrometer. Grain thickness ranged from 250 μm to 1200 μm. Precision was estimated by repeated measurements to be ±3 μm.

Clinopyroxene and orthopyroxene grains of one sample were dehydrated by heating in air at 1000°C for 24 h. Dehydrated mineral mounts were then prepared as described above and used for spectral subtraction.

3.2. Analytical techniques

Quantitative analyses of water in pyroxenes were performed using a Bio-Rad Excalibur FTIR Spectrometer coupled to a UMA-500 microscope. Spectra were obtained with polarized IR light using a KRS5 polarizer (made of thallium bromo-iodide). In order to accurately determine water contents in pyroxenes and other non-isotropic minerals, it is necessary to measure polarized IR spectra on three perpendicular sections of the mineral [24]. In biaxial minerals, it can be measurements made parallel to the principal axes of the optical indicatrix (α, β, and γ). Two grains in appropriate orientations are thus required: either Bxo and Bxa; Bxo and optic-normal; or Bxa and optic-normal. The majority of the spectra in this study were collected from 140×140 μm sample areas using a spectral resolution of 4 cm^{-1} and 64 co-added scans. Smaller sample areas were analyzed in some cases because of restricted polished areas on small mineral grains, or by the necessity to avoid fluid inclusions (italicized values for five clinopyroxene samples in Table 1).

After normalizing each unknown spectrum to 1 mm thickness, the similarly normalized spectrum for the equivalent principal optical axis in the dehydrated mineral was subtracted. The dehydrated spectra come from one sample used as a standard spectrum (one for clinopyroxene, one for orthopyroxene) being subtracted to the pyroxene spectra of all other samples. The following expression of the Beer–Lambert law (H_2O concentration = absorbance/path length × molar absorption coefficient) gives the water content:

$$C_{H2O} = A_i/\mu_i$$

where C_{H2O} is the water concentration in ppm, $A_i = A_\alpha + A_\beta + A_\gamma$, the sum of the areas beneath the O–H stretching vibration absorption peaks in the three perpendicular principal directions of the optical indicatrix normalized to 1 cm thickness (taken between 3750 and 3000 cm^{-1} for clinopyroxene, and between 3750 and 2800 cm^{-1} for orthopyroxene), and μ_i is the integrated molar absorption coefficient (7.09 ppm^{-1} cm^{-2} for clinopyroxene, and 14.84 ppm^{-1} cm^{-2} for orthopyroxene [25]).

Uncertainties come from orientation of the mineral (about ±5°), use of the dehydrated spectra of one standard mineral for background subtraction, including a shift of the background curve of the OH peaks in clinopyroxene due to Fe oxidation during dehydration [25] (~5% 1σ), and 1σ uncertainties of the various terms of the Beer–Lambert law [25], i.e. absorbance measurement (~5%), sample thickness (~0.5%), and absorption coefficient (~5%). Uncertainties (1σ) on individual FTIR measurements are thus estimated to be better than 5%. Analysis of H_2O by FTIR is not a self-calibrating technique. Therefore, a sample of enstatite KBH-1, which had been previously analyzed by both FTIR and manometry [25], was prepared and analyzed as an unknown. The result of 201 ppm H_2O is in good agreement with published analyses (186–217 ppm [25]). Moreover, as much as possible, duplicates, i.e. two different pairs of minerals, were analyzed for the same sample. Reproducibility is better than ±6 ppm for clinopyroxenes and better than ±3 ppm for orthopyroxenes in most cases (Table 1).

4. Results

Water concentrations in clinopyroxene and orthopyroxene were analyzed for 14 samples from

Table 1
Water contents in ppm in orthopyroxene and clinopyroxene, and various petrological parameters for the xenoliths [16,22,23]

Location	Sample	Opx H_2O (ppm)	Cpx H_2O (ppm)	WR Al_2O_3 (wt%)	WR Mg#	T (°C)	P (kbar)	ΔFMQ	Spinel Fe^{3+}/Fe total	Cpx La/Yb
Ventura–Espíritu Santo	SLP-402	187 189	380 413	3.49	88.4	1138	17	−0.01	0.193	0.697
	SLP-400	137 140	n.a.	3.26	82.0	923	12	0.62	0.278	2.166
	SLP-403	243	528	2.98	90.6	1119	20	−1.10	0.043	1.296
	SLP-101	155	398 386	1.56	90.2	1091	22	−0.71	0.140	
	SLP-114	107	221 222	0.68	91.1	1052	14	0.12	0.212	2.682
Santo Domingo	SLP-405	171 162	373	3.50	89.9	1022	14	−1.79	0.029	0.071
	SLP-142	264 280	*514*	2.91	89.8	997	18	−2.19	0.038	0.068
Durango	DGO-166	161 164 166	387 385	3.16	89.8	1091	16	−0.01	0.213	0.142
	DGO-160	86 86	243 254 256	1.12	91.4	1089	16	0.46	0.264	2.558
Mesa Cacaxta	SIN-3	n.a.	*288*	2.87	89.3	1093	14	0.26	0.200	0.141
San Quintin	BCN-200D	186 190	477	3.91	89.2	1042	7	−0.15	0.108	0.331
	BCN-130	124 128	*313*	3.23	88.6	1105	14	0.15	0.262	0.661
	BCN-201B	199 198 203	342	2.58	90.1	1054	12	−0.40	0.139	0.086
	BCN-203	39 38	n.a.	1.81	90.9	1058	13	0.02	0.129	1.882
Simcoe	SIM-9c	71 71	*205*	1.45	92.1	956		0.33	0.270	26.068
	SIM-24	102 115	158	1.32	91.9	969		0.90	0.390	3.728
	SIM-3	109	*140*	1.05	92.2	897		0.78	0.380	7.772
Kilbourne Hole	KBH-1	201 186–217[a]								

Water contents in italics were determined on minerals containing fluid inclusions, but in which a path free of fluid inclusions could be found for the IR beam. n.a. means not analyzed because the minerals contained too many fluid inclusions. WR = whole-rock. Mg# = $Mg/(Mg+Fe^{2+})$.
[a] Values from Bell et al. [25].

Mexico and three samples from Simcoe. Details concerning these samples can be found in Luhr and Aranda-Gómez [16], Brandon et al. [20], and Brandon and Draper [22,23].

OH infrared bands occur between 3750 and 2800 cm^{-1} in pyroxenes (Fig. 2). Spectra of Mexican pyroxenes resemble those obtained from mantle pyroxenes by Bell et al. [25]. The spectra of Simcoe pyroxenes, however, have relatively sharper peaks (less broad bands) at 3540 cm^{-1} and 3460 cm^{-1} in clinopyroxene, and at 3300, 3210, 3060 cm^{-1}, and 3570 cm^{-1} (only β direction) in orthopyroxene. Most clinopyroxene spectra lack the 3355 cm^{-1} band [26], excepting those for Mexican harzburgite SLP-114 and the Simcoe harzburgites. Some bands are poorly resolved at

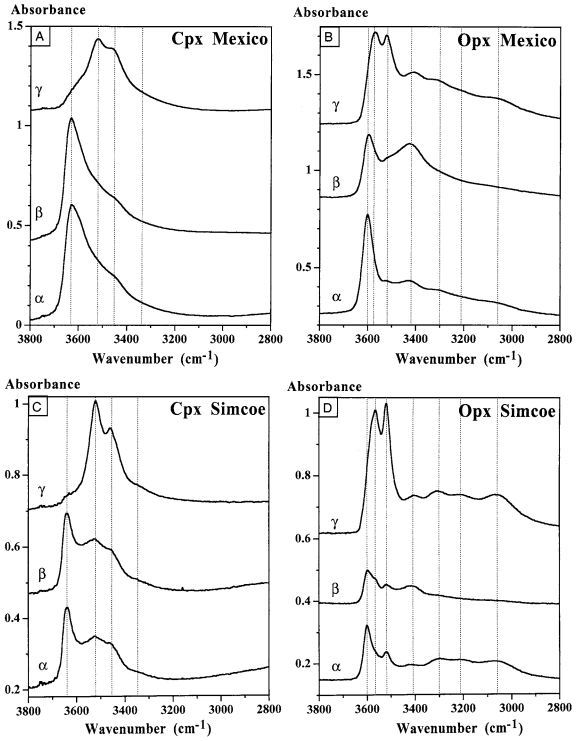

Fig. 2. Typical FTIR spectra of clinopyroxene (Cpx) and orthopyroxene (Opx) in Mexican and Simcoe samples in the O–H stretching frequency range. Spectra are normalized to 1 mm thickness, and the corresponding dehydrated spectrum is subtracted. All three perpendicular directions are shown (corresponding to polarized spectra parallel to the α, β, and γ directions of the pyroxene optical indicatrices). Dotted lines indicate peak locations.

the resolution the spectra were taken (4 cm^{-1}) and are positioned on the tail of stronger bands (for example clinopyroxene 3520 cm^{-1} band in the α and β directions) or are hardly visible (for example orthopyroxene 3060 cm^{-1} in the β direction). Peak heights for the main water absorption bands, however, correlate with one another among all clinopyroxene (or orthopyroxene) spectra, with correlation coefficients (r^2) of 0.82–0.95 (Fig. 3), emphasizing the good quality of the data, and their internal consistency. The fact that these correlations do not project through the origin might reflect the peak overlapping discussed above, as a low-intensity narrow peak overlapping with a high-intensity broad peak would appear more intense than its true intensity. Correlations ($r^2 = 0.4$–0.8) are observed between clinopyroxene peak heights for water absorption bands (Table 2) and a number of clinopyroxene major element concentrations: positive correlations with Ti, Al, Na, and negative correlations with Si, Mg, and Ca (Fig. 4). Correlations of these same parameters for orthopyroxenes are significantly poorer (Fig. 4).

Water concentrations vary from 140 to 528 ppm H_2O in clinopyroxene and from 39 to 265 ppm H_2O in orthopyroxene. These values span the range of previously published water contents in pyroxenes of similar compositions (e.g. [26]). Water content of clinopyroxene correlates with that of orthopyroxene ($r^2 = 0.8$), but at about twice the concentration (Fig. 5). Simcoe water contents are among the lowest analyzed. Orthopyroxene in sample BCN-203 has an anomalously

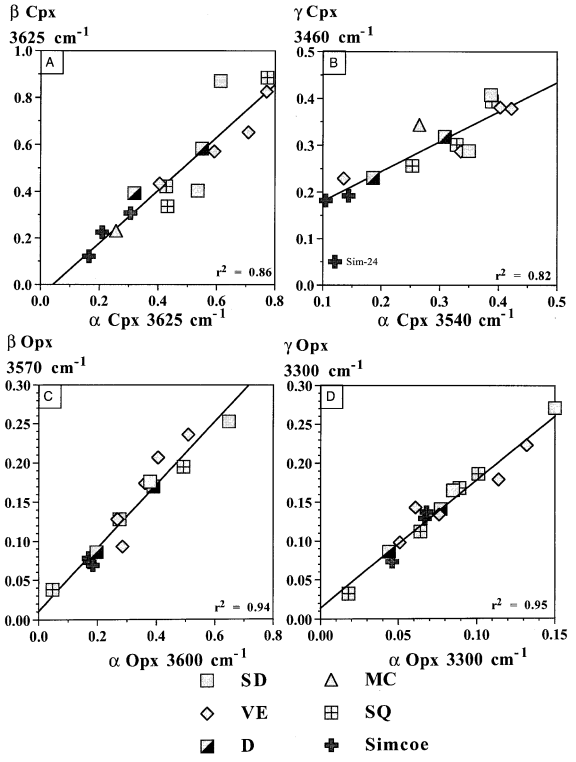

Fig. 3. Examples of correlations between OH peak heights (Table 2) within each spectrum of clinopyroxene (A,B) and orthopyroxene (C,D). The good quality of the correlations ($r^2 = 0.82$–0.95) demonstrates the internal consistency of these FTIR water measurements.

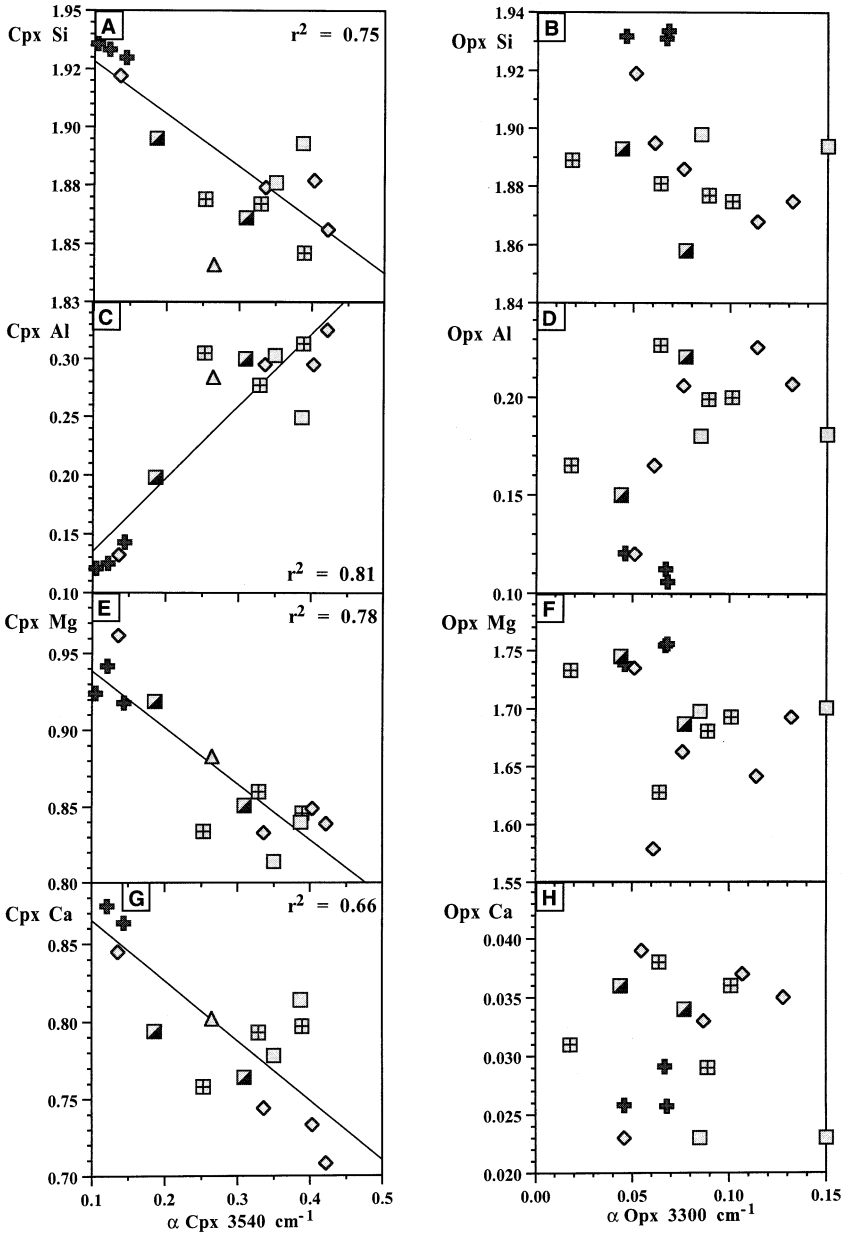

Fig. 4. Correlations between peak heights in the O–H stretching region of the FTIR spectra for clinopyroxene (Cpx) and orthopyroxene (Opx), and pyroxene chemical components (cation units). In A, the plot of α Cpx 3540 cm^{-1} versus Cpx Si, sample SIN-3 was excluded in the calculation of the correlation coefficient ($r^2 = 0.75$). Symbols as in Fig. 3.

low water content of 39 ppm, which makes it plot off any observed correlations between water contents and other parameters, and as such has been excluded from any coefficient of correlation calculation. One of the Mexican samples (SLP-400) has phlogopite as an accessory phase, but the water content of its orthopyroxene is in the middle of the range measured for that mineral (139 ppm H_2O). Among the pyroxene major elements, the best correlations with water contents for both

Table 2
IR absorbance peak heights (in absorbance units) at all O–H stretching frequencies, polarized parallel to the α, β, and γ axes in orthopyroxene and clinopyroxene

Sample		Opx								Cpx				
cm^{-1}		3600	3570	3520	3430	3410	3300	3206	3060	3625	3540	3520	3460	3355
SLP-402	α	0.406	*0.224*	0.144		0.144	0.114	*0.083*	0.049	0.709	0.422		0.286	*0.123*
SLP-400	α	0.268	0.130	0.091	0.069		0.061	*0.048*	0.047					
SLP-403	α	0.509	*0.284*	0.174	0.178		0.132	0.102	0.075	0.771	0.403		0.267	*0.101*
SLP-101	α	0.362	*0.182*	0.107	0.114		0.076	*0.053*	0.041	0.592	0.336		0.209	*0.076*
SLP-114	α	0.285	*0.109*	0.083	0.085		0.051	*0.035*	0.029	0.405	0.136		0.122	*0.057*
SLP-405	α	0.379	*0.201*	0.122	0.110		0.085	0.063	0.044	0.535		0.350	0.185	*0.072*
SLP-142	α	0.648	*0.323*	0.208	0.192		0.150	0.112	0.092	0.613	*0.387*		0.244	*0.089*
DGO-166	α	0.390	0.206	0.112	0.111		0.077	*0.060*	0.047	0.550	*0.309*		0.203	*0.076*
DGO-160	α	0.197	*0.094*	0.062	0.058		0.044	0.032	0.024	0.319	0.186		0.142	0.059
SIN-3	α									0.257		0.265	0.209	*0.077*
BCN-200D	α	0.493	*0.226*	0.131	0.136		0.089	*0.061*	0.045	0.773	*0.389*		0.257	*0.095*
BCN-130	α	0.275	0.157	0.089	0.097		0.064	0.044	0.033	0.428	0.253		0.178	*0.072*
BCN-201B	α	0.394	0.274	0.133	0.130		0.101	0.078	0.057	0.432	0.329		0.211	*0.088*
BCN-203	α	0.047	0.044	0.026	0.015		0.018	0.017	0.011					
Sim-9c	α	0.184	0.081	0.069		0.057	0.046	0.035	0.028	0.306	0.144		0.129	0.061
Sim-24	α	0.174	*0.100*	0.090		0.048	0.067	0.065	0.060	0.210		0.121	0.103	0.022
Sim-3	α	0.170	*0.096*	0.089		0.051	0.068	0.062	0.059	0.165		0.105	0.089	0.031
KBH-1	α	0.464	*0.250*	0.152	0.159		0.110	0.087	0.070					
SLP-402	β	0.280	*0.207*	*0.170*	0.228		*0.107*	0.065	0.035	0.652	0.363		0.248	*0.106*
SLP-400	β	0.201	*0.128*	0.092	0.132		*0.046*	0.022	0.010					
SLP-403	β	0.350	*0.236*	*0.186*	0.255		0.128	*0.084*	0.056	0.826	0.439		0.298	*0.131*
SLP-101	β	0.270	*0.174*	0.133	0.186		0.087	0.053	0.034	0.571	0.290		0.179	*0.060*
SLP-114	β	0.187	*0.093*	*0.086*	0.147		*0.055*	0.032	0.019	0.433	0.135		0.120	0.054
SLP-405	β	0.257	*0.176*	0.134	0.179		*0.085*	0.054	0.034	0.403	0.276		0.153	*0.048*
SLP-142	β	0.426	*0.253*	0.205	0.335			*0.087*	0.053	0.871	*0.451*		0.298	*0.123*
DGO-166	β	0.255	*0.170*	0.129	0.177		0.085	0.057	0.041	0.583	*0.289*		0.191	*0.077*
DGO-160	β	0.139	*0.086*	0.061	0.080		0.035	0.021	0.015	0.392	0.199		0.137	*0.060*
SIN-3	β									0.231		0.206	0.158	*0.055*
BCN-200D	β	0.299	*0.195*	0.159	0.232		0.103	*0.063*	0.040	0.886	*0.372*		0.236	*0.097*
BCN-130	β	0.194	*0.128*	0.097	0.125		0.066	*0.045*	0.031	0.421	0.236		0.171	*0.083*
BCN-201B	β	0.278	*0.190*	0.156	0.225		0.104	*0.067*	0.044	0.336	0.252		0.158	*0.083*
BCN-203	β	0.032	0.038	0.022		0.014	0.010	0.009	0.080					
Sim-9c	β	0.118	0.069	0.052	0.079		0.032	0.018	0.009	0.307	0.136		0.095	0.034
Sim-24	β	0.112	0.073	0.055		0.062	0.030	*0.016*	0.006	0.225		0.145	0.012	0.034
Sim-3	β	0.115	0.078	0.069		0.067	0.034	0.023	0.016	0.121		0.101	0.089	0.043

Table 2 (*Continued*).

Sample		Opx								Cpx				
cm^{-1}		3600	3570	3520	3430	3410	3300	3206	3060	3625	3540	3520	3460	3355
KBH-1	β	0.287	*0.193*	0.141	0.176		0.095	0.064	0.045					
SLP-402	γ	*0.248*	0.424	0.388		0.227	0.179	*0.128*	0.090	0.205		0.414	0.378	*0.137*
SLP-400	γ	*0.197*	0.364	0.395		0.169	0.143	0.113	0.112					
SLP-403	γ	*0.287*	0.477	0.462		0.269	0.223	0.171	0.134	0.130		0.418	0.381	*0.133*
SLP-101	γ	*0.195*	0.298	0.279		0.175	0.134	*0.099*	0.078	0.126		0.313	0.287	0.114
SLP-114	γ	*0.114*	0.176	0.200		0.123	0.098	*0.068*	0.062	0.050		0.198	0.229	0.087
SLP-405	γ	*0.266*	0.398	0.403		0.168	0.165	*0.131*	0.100	0.121		0.410	0.288	*0.094*
SLP-142	γ	*0.379*	0.488	0.567		0.283	0.271	0.208	0.177	0.121		0.468	0.408	0.115
DGO-166	γ	*0.203*	0.345	0.310		0.172	0.141	*0.111*	0.088	0.115		0.365	0.318	*0.104*
DGO-160	γ	*0.135*	0.254	0.220		0.107	0.086	0.063	0.055	0.076		0.246	0.230	0.085
SIN-3	γ									*0.034*		0.479	0.343	*0.104*
BCN-200D	γ	*0.212*	0.340	0.353		0.207	0.168	0.127	0.105	0.118		0.430	0.394	*0.140*
BCN-130	γ	*0.150*	0.286	0.248		0.135	0.112	*0.089*	0.072	0.091		0.290	0.256	*0.082*
BCN-201B	γ	*0.253*	0.411	0.429		0.200	0.186	0.152	0.127	0.091		0.395	0.301	*0.089*
BCN-203	γ	*0.089*	0.247	0.187		0.041	0.032	*0.027*	0.020					
Sim-9c	γ	*0.103*	0.200	0.215		0.084	0.073	0.053	0.052	0.070		0.206	0.192	0.055
Sim-24	γ	*0.195*	0.391	0.411		0.115	0.129	0.116	0.115	0.016		0.282	0.050	0.048
Sim-3	γ	*0.190*	0.338	0.401		0.121	0.137	0.124	0.128	0.033		0.220	0.182	0.055
KBH-1	γ	*0.238*	0.391	0.388		0.215	0.181	0.143	0.120					

Values in italics represent absorbance height measurements where no peaks are visible.

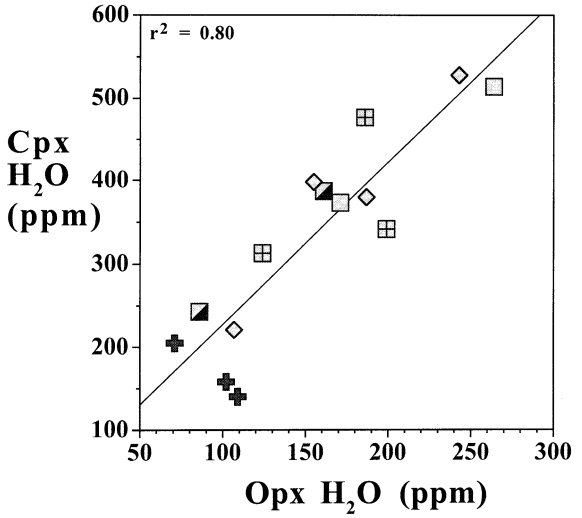

Fig. 5. Orthopyroxene (Opx) and clinopyroxene (Cpx) water contents in ppm H_2O taken from Table 1. Symbols as in Fig. 3.

minerals is for Na, with $r^2 = 0.68$ for clinopyroxene and $r^2 = 0.5$ for orthopyroxene (Fig. 6). Correlations are also observed between pyroxene water contents and whole-rock major elements such as Al_2O_3 (Fig. 7), TiO_2, CaO, Na_2O (positive), and MgO (negative). Negative correlations are present between pyroxene water contents and both spinel $Fe^{3+}/\Sigma Fe$ values and calculated ΔFMQ (Fig. 8), with correlations for clinopyroxene considerably better than for orthopyroxene. In contrast, there are no correlations between pyroxene water contents and calculated temperature, pressure, whole-rock La/Yb, clinopyroxene La/Yb, or distance to the paleotrench.

5. Discussion

5.1. Water incorporation and location in diopside and enstatite

Experiments have shown that water incorporation in pyroxenes depends on the Fe content of the mineral, temperature, pressure, and oxygen fugacity [27–32]. In this study, no clear correlation was observed between FeO and water contents in either clinopyroxene or orthopyroxene. However, two groups can be distinguished, one with high FeO and H_2O (>2.7 wt% and >275 ppm, respectively, for clinopyroxene, and >6 wt% and >115 ppm, respectively, for orthopyroxene) and one with low FeO and H_2O. Exceptions exist, however, most notably in Fe-rich, phlogopite-bearing SLP-400, whose orthopyroxene has 11.3% FeO but only 137 ppm water. Therefore, Fe content of pyroxene does not seem to have been the main control on water incorporation in Mexican and Simcoe pyroxenes. Similarly, water contents in pyroxenes from this

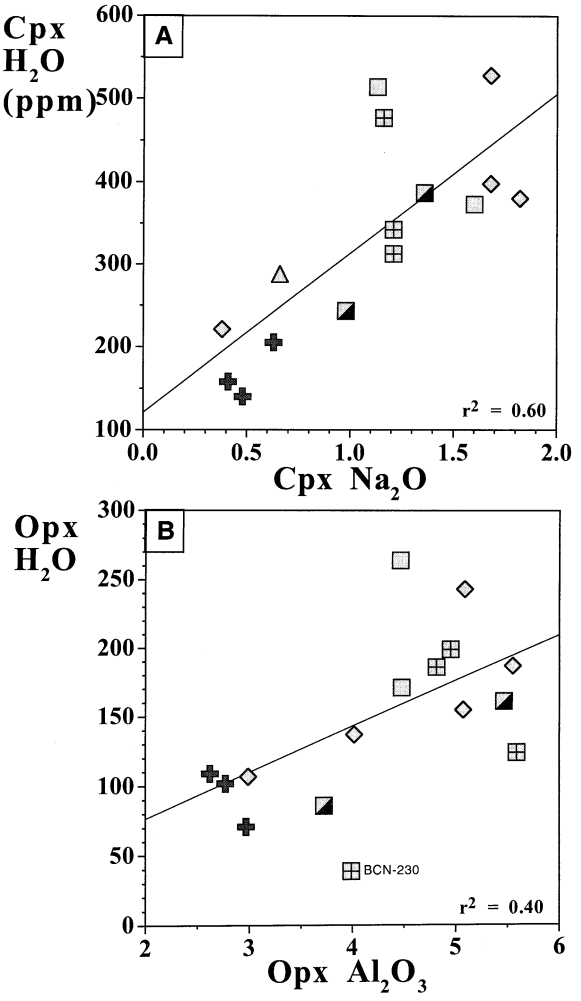

Fig. 6. (A) Na_2O versus ppm H_2O in clinopyroxene. (B) Al_2O_3 versus ppm H_2O in orthopyroxene. Symbols as in Fig. 3.

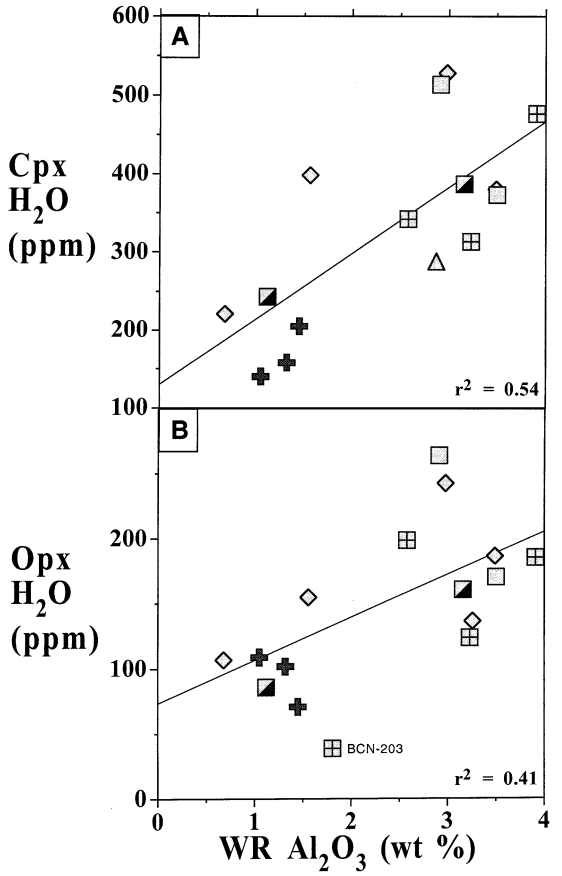

Fig. 7. Whole-rock Al_2O_3 versus (A) clinopyroxene H_2O content and (B) orthopyroxene H_2O content. Symbols as in Fig. 3.

study do not show any relationship to calculated equilibration temperatures or pressures. Oxygen fugacity, as expressed by spinel $Fe^{3+}/\Sigma Fe$ and calculated ΔFMQ values, however, correlates well with pyroxene water contents (Fig. 8). Control of water content in pyroxenes by prevailing oxygen fugacity is also consistent with the mechanism of H incorporation in these minerals, which involves the reduction of iron according to the reaction [29]:

$$Fe^{3+} + O^{2-} + 1/2\ H_2 = Fe^{2+} + OH^-$$

Using peak-height pleochroism, two groups of OH bands have been distinguished in pyroxenes, with group I between 3650 and 3400 cm^{-1} in Opx and between 3700 and 3560 cm^{-1} in Cpx, and group II as the bands at lower wave-numbers [26]. These groups have been interpreted as reflecting more than one type of hydrogen location in pyroxenes ([26], and references therein). Moreover, the stretching frequencies of O–H measured by FTIR between 3200 and 3700 cm^{-1} have been correlated with the distances between H and O atoms in hydrous minerals [33]. If that relationship holds for anhydrous minerals like pyroxenes, it could mean that group I bands reflect shorter O–H bonds than group II bands, i.e. different OH environments. In Mexican and Simcoe peridotites, only the melt-depleted ones (i.e. low whole-rock Al_2O_3) show the low-frequency 3355 cm^{-1} OH bands in clinopyroxene. Furthermore, the most oxidized peridotites such as those from Simcoe have sharper peaks at the lower-frequency range in their pyroxenes than do more reduced and more water-rich peridotites (Fig. 2). It is possible, therefore, that pyroxenes with low water contents, which characterize the most melt-depleted and oxidized peridotites, might have overall stronger, shorter, and/or more consistently oriented O–H bonds than pyroxenes from other environments. It seems reasonable that pyroxenes in an environment that does not favor water incorporation should retain water in the form of the strongest O–H chemical bonds. Differences in the spectra of Mexican and Simcoe pyroxenes may also result from differences in major and trace element chemistry of the pyroxenes; Simcoe pyroxenes are more depleted (Fig. 4) and more light rare earth element enriched [22,23] than the Mexican ones [16] (Table 1).

Indications of exactly where water is incorporated in the structure of pyroxenes might be provided by examining correlations between OH peak heights and concentrations of certain elements. Clinopyroxene group I bands have been associated with trivalent ions [34]. In Mexican and Simcoe clinopyroxenes, however, correlations of Al (or $Al+Cr+Fe^{3+}$) with group II bands are better than with group I bands. Finally, some water peaks in sodic clinopyroxenes [35], and possibly in orthopyroxenes [36], have been associated with cation vacancies. Microprobe analyses, how-

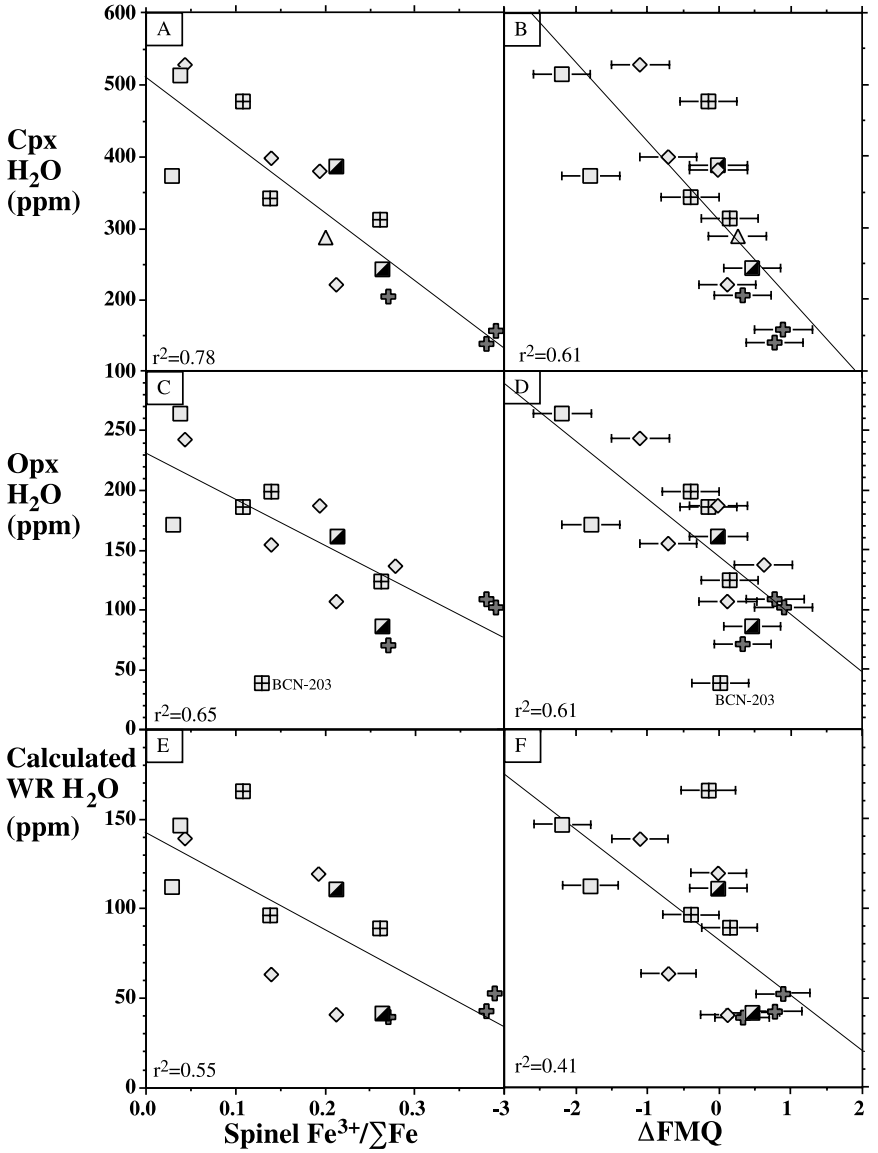

Fig. 8. (Left panel) $Fe^{3+}/\Sigma Fe$ in spinel versus (A) clinopyroxene H_2O content, (C) orthopyroxene H_2O content, and (E) total xenolith H_2O content, assuming 20 ppm H_2O in olivine and no water in spinel, and using the calculated xenolith modes [16,20]. $Fe^{3+}/\Sigma Fe$ in spinel include Mössbauer data for Simcoe samples [20] and calculated values from electron microprobe data in the case of the Mexican samples [16]. Calculation is as follow for the Mexican samples: $Fe^{3+} = 8-(4Ti+3Al+3Cr+2Fe+2Mn+2Ni+2Mg)$ and $Fe^{2+} = Fe+(4Ti+3Al+3Cr+2Fe+2Mn+2Ni+2Mg)-8$ using cation units normalized to three cations. Uncertainty on the Mössbauer $Fe^{3+}/\Sigma Fe$ values is estimated to be ± 0.005 [20], which is smaller than the symbols. (Right panel) Oxygen fugacity expressed as ΔFMQ [56] versus (B) clinopyroxene H_2O content, (D) orthopyroxene H_2O content, and (F) total xenolith H_2O content. Uncertainty on ΔFMQ is estimated to be ± 0.4 log units [16,20].

ever, do not indicate an appreciable abundance of cation vacancies in our samples. On the other hand, OH peak heights correlate positively with elements located in the M1 site (Ti, Al, Mg, Mn), M2 site (Na, Ca, Mg, Mn), and T site (Si) (Fig. 4). This might mean that most OH^- in pyroxenes is at the juncture of these three sites, i.e. replacing an oxygen in position O(2) in the pyroxene struc-

ture [37]. This is consistent with previous findings [35,36] and the fact that the O(2) site in pyroxenes is highly under-bonded [37], making it a likely site for OH^- substitution [34]. The fact that the 3355 cm^{-1} band in clinopyroxene is only present in the most melt-depleted samples (harzburgites) is consistent with the conclusions of Skogby et al. [34].

5.2. Processes controlling pyroxene water contents

5.2.1. Water loss during xenolith transport to the surface?

Dehydration experiments have shown that hydrogen diffuses rapidly in olivine and clinopyroxene [28,31,38]. Concerns have thus been raised that decompression of xenoliths during transport by host magmas to the surface could result in H loss, and that water contents measured in xenolith minerals may underestimate the original mantle abundances [28,31,32,38]. The data for Mexican and Simcoe xenoliths presented in this study, however, demonstrate that this mechanism is not significant. For example, a number of chemical parameters for the minerals and the whole-rock xenoliths that are completely independent of xenolith transport correlate well with the pyroxene water contents. Perhaps most compelling are the correlations between pyroxene water content and whole-rock Al_2O_3 content (Fig. 7). Similarly, Al, Mg, and Ca (Figs. 4 and 6) are essential structural constituents of the pyroxenes and thus are unlikely to be disturbed during the few to dozens of hours that characterize xenolith transport by mafic alkalic magmas to the surface [39]. Spinel $Fe^{3+}/\Sigma Fe$ values (Fig. 8) are also unlikely to be affected by rapid decompression or exchange with the host magma because resetting of trivalent cations in spinel is a very slow process [40]. Finally, incorporation of H in pyroxene depends not only on how fast H diffuses, but also on how fast exchange reactions take place that incorporate H in the mineral structure. These reactions (equilibration of point-defects assumed to be associated with H incorporation such as metal vacancies) are very slow compared to the rates of H diffusion and incorporation into the structure [26]. For example, the time required to re-equilibrate H in a 1–10 mm pyroxene grain at 1000°C is estimated to be over a year [26], which is clearly less than estimated durations of xenolith transport.

5.2.2. Partial melting and H partitioning

Mexican and Simcoe peridotite xenoliths are interpreted as residues from which various percentages of melt have been extracted. The positive correlation between pyroxene water contents and whole-rock indices of partial fusion, such as Al_2O_3 (Fig. 7), indicates that the range of water contents is at least in part due to melting processes. The fact that the most melt-depleted samples (lower Al_2O_3 values) have lower water contents in the pyroxenes of the residue is in agreement with water behaving as an incompatible element during partial melting [41–43]. The significant scatter of data in Fig. 7, however, indicates that partial melting is probably not the only process responsible for these water contents. Finally, clinopyroxene consistently has two times more water than orthopyroxene (Fig. 4), suggesting a partition coefficient of H (D_H) between them of about 2.

5.2.3. Metasomatism and subduction

Pyroxene water contents do not correlate with distance to the paleotrench, indicating that there is no simple relationship between subduction-zone proximity and water contents in nominally anhydrous minerals of the mantle. The clinopyroxene La/Yb values also show no relationship with the pyroxene water contents, and hence, metasomatism interpreted to be responsible for large-ion lithophile element (LILE) enrichment in some of the clinopyroxenes is not correlated with pyroxene water contents. Simcoe clinopyroxenes, however, have higher La/Yb (4–26) and lower water contents compared to the Mexican clinopyroxenes (La/Yb = 0.6–2.6). High H_2O/K_2O in primitive melt inclusions in arc volcanic rocks and ophiolites also indicate that water and LILE can be decoupled during metasomatism [44].

The fact that pyroxene water contents are lowest when the oxygen fugacity (ΔFMQ) and spinel $Fe^{3+}/\Sigma Fe$ values are highest (Fig. 8) suggests that the oxidation state of the mantle is controlling the amount of water present in pyroxenes. It implies that the solubility of water in pyroxene is negatively correlated with oxygen fugacity. Only one

experimental study of H incorporation into clinopyroxene [30] included the effect of variable oxygen fugacity, and showed that a synthetic clinopyroxene under low fO_2 conditions (1.2 log fO_2 below the Fe–FeO solid buffer) incorporated more H than one under high fO_2 conditions (FeO–Fe_3O_4 solid buffer), consistent with the trends of Fig. 8.

Typically, island-arc basalts and their mantle xenoliths record relatively high oxygen fugacities [45–47]. Simcoe xenoliths are samples of a mantle wedge that developed along a continental margin, and they record very high oxygen fugacities [18,20], and low pyroxene water contents (Fig. 8). Mexican samples have a wide range of oxygen fugacities that are, when averaged, higher and less variable for the xenolith locations closer to the paleotrench [16]. Lattard [17] has challenged this observation. She argued that the pressure dependence inherent in ΔFMQ values makes the postulated SE–NW trend of questionable significance. Nonetheless, when relative oxidation is expressed in the preferable form ΔNNO (relative to the Ni–NiO buffer), values for the xenoliths from the NW fields (MC and SQ in Fig. 1) are still systematically higher than values for xenoliths from the SE fields (VE, and especially SD). Lattard [17] also discounts the interpretation that metasomatism is associated with oxidation, emphasizing that rocks metasomatized by oxidized fluids/melts would show elevated whole-rock $Fe^{3+}/\Sigma Fe$, but not necessarily record increased oxygen fugacities. She also acknowledges that debate still exist on the matter. The fact, however, that water contents in pyroxenes measured by FTIR correlate clearly with spinel $Fe^{3+}/\Sigma Fe$ and whole-rock ΔFMQ, estimated using microprobe data for Mexico and Mössbauer data for Simcoe samples, indicates that these oxidation trends are real. As demonstrated for the Simcoe samples [20,22,23], the low pyroxene water contents in the most oxidized Mexican samples also suggest that the water–oxidation correlation is related to subduction.

The reason why the mantle wedge is more oxidized than other parts of the mantle is a matter of debate. Metasomatism by oxidizing fluids or melts is the most likely explanation, but these metasomatic agents could be either hydrous fluids, silicate melts, or supercritical fluids at the source depths for the Mexican and Simcoe spinel-peridotite xenoliths [20,47,48]. No experimental results are available for water partitioning between minerals and these possible metasomatic phases in the spinel stability field, and extrapolation from data for simple synthetic systems at higher pressure [49] is not possible due to the extreme differences in phase compositions and structures. Earlier studies of the Simcoe xenoliths pointed towards an oxidized, water- and alkali-rich melt as the metasomatic medium [20,22,23]. Infiltration of such a melt would likely induce partial melting of the peridotite. The Simcoe harzburgites, residues of this partial melting process, would probably have equilibrated with the oxidized melt, and based on the negative relationship between oxygen fugacity and H solubility in pyroxene, they would have lost roughly half of their H to the melt. This equilibration was probably not related to a discrete melt infiltration event, but rather the cumulative effect of many millions of years of a continuous percolation of oxidizing fluids/melts from the slab and from its hybridized hanging wall [23].

If subduction-related high-fO_2 metasomatism results in release of water from the mantle-wedge pyroxenes, an obvious question arises: where does that water go? We first examine the possibility that small domains of the peridotite act as closed systems, with the water re-partitioned among existing phases. Of the two other anhydrous minerals in peridotite, spinel does not incorporate any significant water [50], and olivine can hold only very small amounts, typically less than 50 ppm [6,43,51,52]. Moreover, it can be speculated that water contents in olivines from Simcoe and Mexican peridotites will parallel those in pyroxenes, because the mechanism of H incorporation into olivine is the same as that for pyroxenes (see above, and [38]). Water contents for the whole-rock peridotites were calculated assuming a constant water content for olivine of 20 ppm for all samples and using the mineral modes of the xenoliths. The whole-rock values also correlate negatively with oxygen fugacity (Fig. 8F). Thus, repartitioning of the water on a closed-system basis

does not appear to be a viable explanation, unless newly formed hydrous phases are created.

Another possible explanation is that the water is held by newly formed hydrous minerals or glass in the mantle, either in closed system re-equilibration or in response to an influx of metasomatic fluids or melts. At Simcoe, minor phlogopite was noted in two of five xenoliths studied by Draper [18]. In Mexico, phlogopite was present in one studied sample (SLP-400) from the Ventura field, which is the most distant from the paleotrench. The peridotite xenoliths from other Mexican locations do not have any hydrous minerals [16], however, casting doubt on this explanation for the 'missing' water. Glass was observed in all Mexican xenoliths [16], as well as in some of the Simcoe xenoliths [18]. Glass presence thus seems independent of pyroxene water content.

A third possibility is that the water migrates out of the mantle-wedge pyroxenes into percolating metasomatic fluids and/or melts produced by partial melting of the peridotite. Silica- and alkali-rich glasses that are common along grain boundaries in peridotites from Mexico [16], Simcoe [18], and worldwide localities [53] could also be remnants of these percolating melts. Phlogopite-bearing SLP-400, and the similar phlogopite-bearing Simcoe peridotites described by Draper [18], could represent more extreme examples of this process. They contain veinlets of phlogopite, glass, and other minerals cutting across the peridotites textures, evidence of infiltration by late-stage hydrous melts. SLP-400 and the Simcoe peridotites record the highest ΔFMQ values in this study, and show some of the lowest pyroxene water contents. We interpret these observations as follows. Prior to the start of subduction, the peridotites were free of phlogopite-bearing veinlets, and had low ΔFMQ values (−1 to −2) and high pyroxene water contents (∼500 ppm in clinopyroxene and ∼275 ppm in orthopyroxene, Fig. 5). Oxidized metasomatic fluids or melts later rose from the subducting slab, invaded the overlying mantle-wedge peridotites, and equilibrated with them. This induced melting in the peridotites, raised ΔFMQ values, lowered the solubility of H in pyroxenes, and extracted roughly half of the pyroxene H into the melt, from which phlogopite was precipitating. A similar process may operate in most sub-arc mantle-wedge peridotites, although many may not reach the extreme melt water contents to cause precipitation of phlogopite. Through this process, sub-arc mantle-wedge peridotites become oxidized and their pyroxenes become H depleted. The H extracted from peridotitic pyroxenes, the water that rose from the subducting slab in the form of metasomatic fluids, and the silicate melts that were induced through fluxing of the peridotites by the metasomatic fluids, combine to form the water-rich and oxidized basaltic melts that are parental to the calc-alkaline magmas dominant in subduction zones. In this sense, the low water contents of pyroxenes in sub-arc mantle-wedge peridotites might be complementary to the high magmatic water contents and explosive eruptions that characterize subduction-zone volcanoes.

5.2.4. Water budget in subduction zones

If peridotite minerals in the sub-arc mantle wedge lose water during oxidation by subduction-related fluids or melts, what fraction of the water content of the subduction-related magmas does that represent? In order to make that estimation, we assume a simple model for a subduction zone; a slab dipping at 45°, an overlying mantle wedge extending 300 km horizontally from the trench, by 1 km strike length (parallel to the trench), and a 30 km thick crust. This simple model is a good representation of the subduction zones beneath Simcoe [54] and western Mexico [55]. With this geometry, the volume of mantle-wedge peridotite is 36 450 km^3. With a density of 3400 kg m^{-3}, this corresponds to 1.24×10^{17} kg of peridotite. From the results of this study, a peridotite that typically has about 150 ppm water represents the mantle unaffected by arc metasomatism and brought in the region by tectonic cycling of the mantle wedge. This peridotite loses about two thirds of its water, i.e. about 100 ppm, after undergoing the amount of oxidation recorded in the Simcoe xenoliths (Fig. 8). Assuming that our entire mantle-wedge slice has been affected by such metasomatism, it represents a total loss of 1.24×10^{13} kg water. If we further assume that the subduction zones at

Simcoe and western Mexico were active for about 50 Ma, and that the flux and consequent metasomatism of the mantle wedges were both continuous and uniformly distributed, a water loss of 2.48×10^5 kg per year is calculated for the model slice. In comparison, worldwide total water flux in subduction-zone magmas has been estimated to be 1.4×10^{11} kg per year [1]. Knowing that subduction strike length worldwide is about 30 000 km (P.G. Silver in [20]), the amount of water carried in arc magmas per year per 1 km strike length unit is 4.7×10^6 kg. According to these calculations, the water loss by dehydration of peridotite minerals in the mantle wedge represents at most 5% of the total water in arc magmas. Because metasomatism by oxidized fluids or melts is likely to be neither continuous in time nor homogeneous in space, the amount of water released by mantle-wedge pyroxenes may represent much less than 5% of total arc magma water. In particular, the calculation above assumes that: (1) all of the mantle wedge has been oxidized, (2) the level of oxidation everywhere has been maximum (i.e. 3.5 ΔFMQ unit shift, Fig. 8), (3) these phenomena resulted in a constant water loss that was taken as our maximum value, 100 ppm H_2O, and (4) the mantle-wedge peridotite is not being renewed through passive flow over the period of time considered.

Although the conclusions above are limited by the uncertainties associated with the many assumptions made in the calculation, they still indicate that more than 95% of the water released by arc magmas does not come from dehydration of anhydrous minerals in the mantle wedge. An important corollary is that water in arc magmas mainly comes from fluids or melts derived from the slab itself. The peridotite of the mantle wedge acts more as an easy medium for water to be transported to the surface by arc magmas, rather than being a major contributor in the subduction-zone water budget.

6. Conclusions

The FTIR analyses presented in this paper show that there is less water in pyroxenes from sub-arc mantle-wedge peridotites than in those from peridotites in other parts of the lithospheric mantle in the spinel stability field. The low water contents of these mantle-wedge pyroxenes is thought to be a result of oxidation of the mantle above subduction zones by slab-derived metasomatic fluids/melts. Of the water in the subducted slab that is released beneath the zone of arc magmatism, some poorly constrained fraction is likely stored as amphibole and phlogopite in the down-dragged base of the mantle wedge. The remainder probably percolates upward from the slab, oxidizing the mantle-wedge peridotites and inducing them to partially melt. Oxidation of the mantle-wedge peridotites may significantly lower the solubility of water in their pyroxenes, causing more than half of the water originally housed in the mantle wedge to be expelled. That water is incorporated into the ascending hydrous partial melts that feed the overlying magmatic arc. The nominally anhydrous minerals in the mantle-wedge are not an important storage reservoir for subducted water. Instead the mantle wedge appears to be capable of efficiently transporting slab-derived water to the upper crustal magmatic arc, to which it may contribute up to 5% of the magmatic water. The relatively dry nature of oxidized sub-arc mantle-wedge peridotites can be viewed as a complement to the hydrous and oxidized magmas whose common explosive eruptions characterize subduction-related volcanoes.

Acknowledgements

We thank Tim McCoy for dehydrating minerals for us in his 1-atmosphere furnaces, Tim Gooding for the many hints and help he provided in sample preparation, George Rossman who provided us with the first insights on how to orient and polish our minerals, and David Bell who gave us sample KBH-1 and kindly discussed with us problems associated with water analysis by FTIR. We are also very grateful to Alan Brandon who provided us with the Simcoe samples and whose insights greatly enhanced the quality of this study. We are grateful to Craig Bina for reviewing an earlier version of the manuscript. This

paper benefited greatly from reviews by H. Sgogby, M. Hirschmann and an anonymous reviewer, and editing by B. Wood. This work was in part supported by a Smithsonian Fellowship to A.H.P., NSF Grant EAR 9804909 to A. Brandon, and the Sprague Fund of the Smithsonian Institution.*[BW]*

References

[1] S.M. Peacock, Fluid processes in subduction zones, Science 248 (1990) 329–337.
[2] Y. Tatsumi, Migration of fluid phases and genesis of basalt magmas in subduction zones, J. Geophys. Res. 94 (1986) 4697–4707.
[3] A.B. Thompson, Water in the Earth's upper mantle, Nature 358 (1992) 295–302.
[4] J.R. Smyth, T. Kawamoto, Wadsleyite II: a new high pressure hydrous phase in the peridotite-H_2O system, Earth Planet. Sci. Lett. 146 (1997) E9–R16.
[5] T. Inoue, H. Yurimoto, Y. Kudoh, Hydrous modified spinel, $Mg_{1.75}SiH_{0.5}O_4$: a new water reservoir in the mantle transition region, J. Geophys. Res. 22 (1995) 117–120.
[6] D.R. Bell, G.R. Rossman, Water in Earth's mantle the role of nominally anhydrous minerals, Science 255 (1992) 1391–1397.
[7] J. Chen, T. Inoue, D.J. Weidner, Y. Wu, T. Vaughan, Strength and water weakening of mantle minerals, olivine, wadsleyite and ringwoodite, Geophys. Res. Lett. 25 (1998) 575–578.
[8] S.J. Mackwell, D.L. Kohlstedt, M.S. Paterson, The role of water in the deformation of olivine single crystals, J. Geophys. Res. B 13 (1985) 11319–11333.
[9] J.R. Goldsmith, Al/Si interdiffusion in albite: effect of pressure and the role of hydrogen, Contrib. Mineral. Petrol. 95 (1987) 311–321.
[10] S. Karato, The role of hydrogen in the electrical conductivity of the upper mantle, Nature 347 (1990) 272–273.
[11] S. Karato, H. Jung, Water, partial melting and the origin of the seismic low velocity and high attenuation zone in the upper mantle, Earth Planet. Sci. Lett. 157 (1998) 193–207.
[12] I. Kushiro, Partial melting of mantle wedge and evolution of island arc crust, J. Geophys. Res. B 10 (1990) 15929–15939.
[13] G.A. Gaetani, T.L. Grove, W.B. Bryan, The influence of water on the petrogenesis of subduction-related igneous rocks, Nature 365 (1993) 332–334.
[14] T. Inoue, Effect of water on melting phase relations and melt composition in the system Mg_2SiO_4-$MgSiO_3$-H_2O up to 15 GPa, Phys. Earth Planet. Inter. 85 (1994) 237–263.
[15] F.A. Frey, M. Prinz, Ultramafic inclusions from San Carlos, Arizona: petrologic and geochemical data bearing on their petrogenesis, Earth Planet. Sci. Lett. 38 (1978) 129–176.
[16] J.F. Luhr, J.J. Aranda-Gómez, Mexican peridotite xenoliths and tectonic terranes: correlations among vent location, texture, temperature, pressure and oxygen fugacity, J. Petrol. 38 (1997) 1075–1112.
[17] D. Lattard, Comment on 'Mexican peridotite xenoliths and tectonic terranes: correlations among vent location, texture, temperature, pressure, and oxygen fugacity' by J.F. Luhr and J.J. Aranda-Gomez (1997), J. Petrol. 42 (2001) 847–851.
[18] D.S. Draper, Spinellherzolite xenoliths from Loreta Butte, Simcoe Mountains, southern Washington (USA), J. Geol. 100 (1992) 766–776.
[19] R.P. Riddihough, Recent movements of the Juan de Fuca plate system, J. Geophys. Res. 89 (1984) 6980–6994.
[20] A.D. Brandon, D.S. Draper, Constraints on the origin of the oxidation state of mantle overlying subduction zones: an example from Simcoe, Washington, USA, Geochim. Cosmochim. Acta 60 (1996) 1739–1749.
[21] A.D. Brandon, D.S. Draper, Reply to the comment by B.R. Frost and C. Ballhaus on 'Constraints on the origin of the oxidation state of mantle overlying subduction zones an example from Simcoe, Washington, USA', Geochim. Cosmochim. Acta 62 (1998) 333–335.
[22] A.D. Brandon, R.A. Creaser, S.B. Shirey, R.W. Carlson, Osmium recycling in subduction zones, Science 272 (1996) 861–864.
[23] A.D. Brandon, H. Becker, R.W. Carlson, S.B. Shirey, Isotopic constraints on time scales and mechanism of slab material transport in the mantle wedge: evidence from the Simcoe mantle xenoliths, Washington, USA, Chem. Geol. 160 (1999) 387–408.
[24] E. Libowitzky, G.R. Rossman, Principles of quantitative absorbance measurements in anisotropic crystals, Phys. Chem. Min. 23 (1996) 319–327.
[25] D.R. Bell, P.D. Ihinger, G.R. Rossman, Quantitative analysis of trace OH in garnet and pyroxenes, Am. Mineral. 80 (1995) 465–474.
[26] J. Ingrin, H. Skogby, Hydrogen in nominally anhydrous upper-mantle minerals: concentration levels and implications, Eur. J. Mineral. 12 (2000) 543–570.
[27] J. Ingrin, K. Latrous, J.C. Doukhan, N. Doukhan, Water in diopside: an electron microscopy and infrared spectroscopy study, Eur. J. Mineral. 1 (1989) 327–341.
[28] J. Ingrin, S. Hercule, T. Charton, Diffusion of hydrogen in diopside: results of dehydration experiments, J. Geophys. Res. 100 (1995) 15489–15499.
[29] H. Skogby, G.R. Rossman, OH^- in pyroxene: an experimental study of incorporation mechanisms and stability, Am. Mineral. 74 (1989) 1059–1069.
[30] H. Skogby, OH incorporation in synthetic clinopyroxene, Am. Mineral. 79 (1994) 240–249.
[31] S. Hercule, J. Ingrin, Hydrogen in diopside: diffusion, kinetics of extraction-incorporation, and solubility, Am. Mineral. 84 (1999) 1577–1587.

[32] S. Carpenter Woods, S. Mackwell, D. Dyar, Hydrogen in diopside: Diffusion profiles, Am. Mineral. 85 (2000) 480–487.
[33] E. Libowitzky, Correlation of O-H stretching frequencies and O-H..O hydrogen bond lengths in minerals, Mh. Chem. 130 (1999) 1047–1059.
[34] H. Skogby, D.R. Bell, G.R. Rossman, Hydroxide in pyroxene: variations in the natural environment, Am. Mineral. 75 (1990) 764–774.
[35] J.R. Smyth, D.R. Bell, G.R. Rossman, Incorporation of hydroxyl in upper-mantle clinopyroxenes, Nature 351 (1991) 732–735.
[36] A. Beran, J. Zemann, The pleochroism of a gem-quality enstatite in the region of the OH stretching frequency, with a stereochemical interpretation, Tschermaks Mineral. Petrol. Mitt. 35 (1986) 19–25.
[37] M. Cameron, J.J. Papike, Crystal chemistry of silicate pyroxenes, in: C.T. Prewit (Ed.), Pyroxenes, Rev. Mineral. 7 (1980) 5–92.
[38] S.J. Mackwell, D.L. Kohlstedt, Diffusion of hydrogen in olivine: implications for water in the mantle, J. Geophys. Res. 95 (1990) 5079–5088.
[39] F.J. Spera, Dynamics of translithospheric migration of metasomatic fluids and alkaline magma, in: M.A. Menzies, C.J. Hawkesworth (Ed.), Mantle Metasomatism, Academic Press, London, 1987, pp. 1–20.
[40] C. Ballhaus, R.F. Berry, D.H. Green, High pressure experimental calibration of the olivine-orthopyroxene-spinel oxygen geobarometer: implications for the oxidation state of the upper mantle, Contrib. Mineral. Petrol. 107 (1991) 27–40.
[41] J.E. Dixon, E. Stolper, J.R. Delaney, Infrared spectroscopic measurements of CO_2 and H_2O in Juan de Fuca basaltic glasses, Earth Planet. Sci. Lett. 90 (1988) 87–104.
[42] P.F. Dobson, H. Skogby, G.R. Rossman, Water in boninite and coexisting orthopyroxene: concentration and partitioning, Contrib. Mineral. Petrol. 118 (1995) 414–419.
[43] M. Kurosawa, H. Yurimoto, S. Sueno, Patterns in the hydrogen and trace element compositions of mantle olivines, Phys. Chem. Min. 24 (1997) 385–395.
[44] A.V. Sobolev, M. Chaussidon, H_2O concentrations in primary melts from supra-subduction zones and mid-ocean ridges: implications for H_2O storage and recycling in the mantle, Earth Planet. Sci. Lett. 137 (1996) 45–55.
[45] B.J. Wood, L.T. Bryndzia, K.E. Johnson, Mantle oxidation state and its relationship to tectonic environment and fluid speciation, Science 248 (1990) 337–345.
[46] C. Ballhaus, Redox states of lithospheric and asthenospheric upper mantle, Contrib. Mineral. Petrol. 114 (1993) 331–348.
[47] I.J. Parkinson, R.J. Arculus, The redox state of subduction zones: insights from arc-peridotites, Chem. Geol. 160 (1999) 409–424.
[48] H. Bureau, H. Keppler, Complete miscibility between silicate melts and hydrous fluids in the upper mantle: experimental evidence and geochemical implication, Earth Planet. Sci. Lett. 165 (1999) 187–196.
[49] N. Bolfan-Casanova, H. Keppler, D.C. Rubie, Water partitioning between nominally anhydrous minerals in the MgO-SiO_2-H_2O system up to 24 GPa: implications for the distribution of water in the Earth's mantle, Earth Planet. Sci. Lett. 182 (2000) 209–221.
[50] D.R. Bell, Water in mantle minerals, Nature 357 (1992) 646–647.
[51] G.H. Miller, G.R. Rossman, G.E. Harlow, The natural occurrence of hydroxyde in olivine, Phys. Chem. Min. 14 (1987) 461–472.
[52] G.R. Rossman, Studies of OH in nominally anhydrous minerals, Phys. Chem. Min. 23 (1996) 299–304.
[53] P. Schiano, R. Clocchiatti, Worldwide occurrence of silica-rich melts in sub-continental and sub-oceanic mantle minerals, Nature 368 (1994) 621–624.
[54] M.B. Bostock, J.C. VanDecar, Upper mantle structure of the northern Cascadia subduction zone, Can. J. Earth Sci. 32 (1994) 1–12.
[55] A.W. Bally, A.R. Palmer, (Eds.), The Geology of North America; An Overview, vol. A, The Geological Society of America, Boulder, CO, 1989, 619 pp.
[56] B.J. Wood, D. Virgo, Upper mantle oxidation state: ferric iron contents of lherzolite spinels by 57 Mössbauer spectrometry and resultant oxygen fugacities, Geochim. Cosmochim. Acta 53 (1989) 1277–1291.